

Incipience of quantum chaos in the Jahn-Teller model

Eva Majerníková^{1,2,*} and Serge Shpyrko^{2,†}

¹*Institute of Physics, Slovak Academy of Sciences,
Dúbravská cesta 9, SK-84 511 Bratislava, Slovak Republic*

²*Department of Theoretical Physics, Palacký University,
Tř. 17. Listopadu 50, CZ-77207 Olomouc, Czech Republic*

(Received 26 September 2005; Revised 16 February 2006; Published 24 June 2006)

We studied complex spectra of a two-level electron system coupled to two phonon (vibron) modes represented by the $E \otimes e$ Jahn-Teller model. For particular rotation quantum numbers we found a coexistence of up to three regions of the spectra, (i) the dimerized region of long-range ordered (extended) pairs of oscillating levels, (ii) the short-range-ordered (localized) "kink lattice" of avoiding levels, and (iii) the intermediate region of kink nucleation with variable range of ordering. This structure appears above a certain critical line as a function of interaction strength. The level clustering and level avoiding generic patterns reflect themselves in several intermittent regions between up to three branches of spectral entropies. Linear scaling behavior of the widths of level curvature probability distributions provides the conventionally adopted indication for the presence of quantum chaos. Level spacing probability distributions show peculiarities of the partial (for fixed quantum angular momentum) as well as of the cumulative (all angular momenta) case. The clustering of levels with two and three dominant spacings at fixed angular momenta causes notable deviations of the cumulative distributions from the Poissonian one.

PACS numbers: 05.45.Mt, 31.30.-i, 63.22.+m

I. INTRODUCTION

Generally, a multitude of avoided crossings in complex spectra of a quantum system is considered as the signature of chaos which appears in a quasiclassical limit of the respective nonlinear many-body system with repulsive interactions [1, 2]. In solid-state physics, quantum chemistry, or quantum optics investigations of complex excited energy spectra of models with two electron levels coupled with one or more boson modes are of special relevance for understanding experimental – e.g., optical or transport-properties.

Numerical investigations of the excited spectra of certain two-level one- and two-boson systems [e.g., exciton [3, 4] and $E \otimes e$ Jahn-Teller (JT) model [5]] show the existence of level avoidings and related highly excited "exotic" (localized) states. Signatures of chaos in two-level boson systems remain objects of interest since the early studies by Hamiltonian methods [6, 7, 8, 9, 10, 11]. Later on statistical methods based on the random matrix theory – e.g., level spacing and level curvature probability distributions – were applied mostly for one-phonon-mode models. The level spacing distributions show irregular behavior between the limiting Poisson (regular) and Wigner (fully chaotic) distributions [12, 13, 14, 15]. Specifically, among the level spacing distributions of the two-level one-phonon model [12, 13, 14] there appeared M-shaped distributions with two symmetric peaks for two

dominant spacings. Such distributions are a signature of level clustering (dimerization).

The most familiar representative of the two-level two-phonon models is the $E \otimes e$ JT model [16] with linear coupling to phonon (vibron) modes of different parity against reflection. This model is a prototype for phonons removing the degeneracy of electron levels by an interaction with the antisymmetric phonon mode and *tunneling between the levels assisted by the symmetric phonon mode* (in the one-phonon case the tunneling is purely resonant). The presence of two-phonon modes with equal coupling strengths imposes additional rotational symmetry to the model. Differences between the one-mode two-level phonon model and two-mode JT models become evident when one compares their dimensionality after elimination of the electron (level) degrees of freedom: while in the first case the reduction results in a one-dimensional nonlinear (with self-interaction) quantum oscillator, in the two-mode JT cases the elimination yields a two-dimensional quantum oscillator with nonlinear coupling of its components. While in the one-boson-mode case one finds correlations of two sets of excited states, in the two-boson-mode case mixing of up to three sets takes place depending on the range of parameters. As we show, this leads to the appearance of a third peak in the level spacing distribution (trimerization) for the respective range of parameters.

Recently, Yamasaki *et al.* [17] for the first time investigated the possibility of chaos in spectra of the $E \otimes e$ JT model. Their analysis was based on the approximation of the Hamiltonian by the adiabatic "Mexican hat" potential. Additionally the Hamiltonian was supplemented by an explicit term with nonlinear mode coupling of a trigonal symmetry in order to simulate the effects of fluctuations and nonintegrability. Thus, non-

*Electronic address: fyziemar@savba.sk

†e-mail:serge.shp(at)yahoo.com; On leave from Institute for Nuclear Research, Ukrainian Academy of Sciences, pr.Nauki 47 Kiev, Ukraine

linearity was included via mode coupling in addition to the mean-field bare part of the Hamiltonian. The authors concluded that quantum chaos reflects itself in the Wigner-type level spacing distribution as a consequence of the said nonlinearity of the Hamiltonian. Meanwhile, for the linear part an absence of such patterns was stated. Those conclusions were confirmed at the classical level as well. It is to be noted here that the way of passing to a semiclassical approximation in spin-boson systems is not unique and presents an essential ambiguity from different possible ways of decoupling [6]. Different ways of performing a semiclassical approximation are known to lead to different answers concerning the chaotic behavior of the system. This ambiguity means that a classical analog of such a model is not well defined and cannot be a reliable object in exploring the quantum chaos issues.

In this paper we investigate the characteristics of excited (quasi continuum) spectra of $E \otimes e$ JT model. The present approach differs from that by Yamasaki *et al.* in the following: (a) we *do not* introduce explicit nonlinearity into the initial Hamiltonian. However, its $SU(2)$ symmetry involves an *intrinsic nonlinearity* which is revealed by exact elimination of the electronic degrees of freedom [18]. (b) We start from the $E \otimes (b_1 + b_2)$ model with different coupling strengths for both modes. The rotation-symmetric $E \otimes e$ model represents its particular case with equal coupling constants and thus with the symmetry of a higher (rotational) symmetry group (the difference of the coupling constants in realistic systems is likely to be caused, for example, by spatial anisotropy of crystals). The importance of starting from a more general situation is evident from the nature of quantum fluctuations. Namely, the variational approach to the $E \otimes (b_1 + b_2)$ model used for the calculation of the ground state [18] yielded the largest deviations just for the rotation-symmetric case. In the ground state the abrupt change of energy at equal couplings is an artefact of the adiabatic approximation: the energy region of the quantum $E \otimes e$ model is situated within a smeared border around $\beta/\alpha = 1$ (α and β being the coupling strengths of the antisymmetric and symmetric modes, respectively) between the "selftrapping" ($\alpha > \beta$) and "tunneling" ($\alpha < \beta$) part of the ground state of the model with broken rotational symmetry. In the smeared transition region both phases coexist and are quantum correlated (entangled) via nonlinear correlations between the modes. There the phonon-assisted (by the symmetric mode) tunneling contribution to the energy (from the admixture of two reflection symmetric levels in the excitation reflection Ansatz for the variational wave function[18]) causes an essential decrease of the ground state energy because of changing parity of the wave function by the reflection operator and results in the vanishing of the Ham factor. The phase transition at $\alpha = \beta$ to the rotational symmetry phase provides a representation by the additional rotational quantum number j . We will show that at a given j in $E \otimes e$ model analogous phonon assisted tunneling between adjacent excited levels occurs and is responsible for

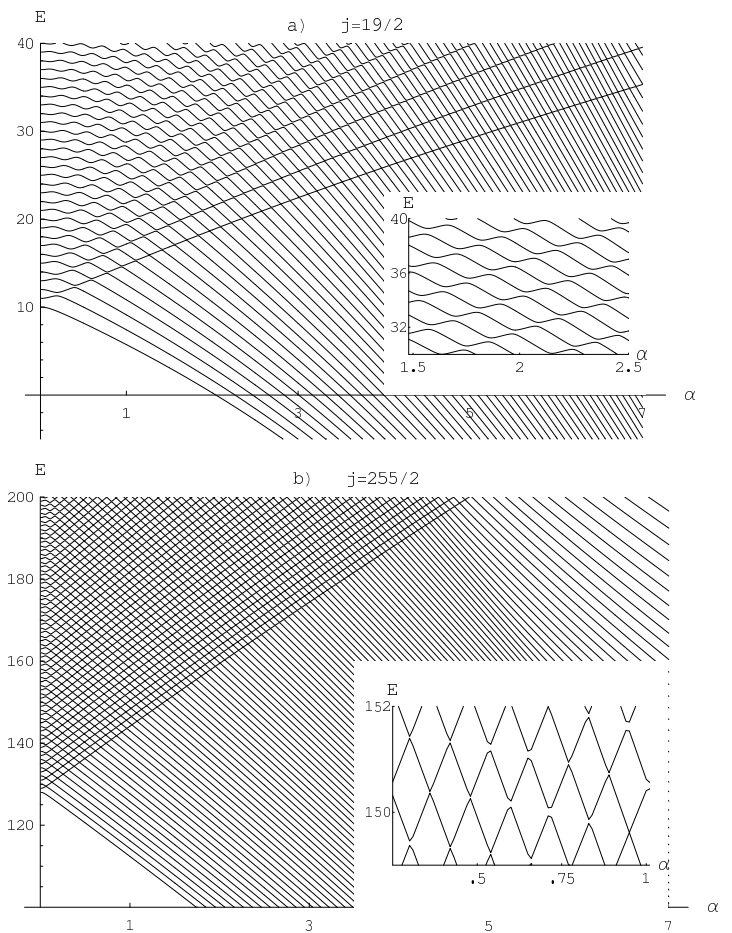


FIG. 1: Energy spectra for $j = 19/2, 255/2$ as a function of α .

the flip (kink) between the levels [this mechanism can be well recognized, e.g., in Fig.1(b)]. This nonlinear effect causes a mixture of the adjacent (even and odd) levels at stronger couplings and leads to nucleation of the new kink lattice phase when increasing the coupling constant. Naturally, the tunneling mechanism due to short-range quantum fluctuations at large j is then the origin of the peculiar irregular behavior of related level spacing distributions and does not allow for full developing of Wigner chaos. The phonon-assisted tunneling and nucleation of the kink lattice phase can also be demonstrated within the formalism of a Calogero-Moser gas of pseudoparticles with repulsive interaction [19, 20].

In Sec. II we briefly present an analytical formulation of the eigenvalue problem in radial coordinates. Since the literature on one-phonon models is more abundant and certain similarities between both models appear, it is useful to point out the essential differences based on a comparison of the relevant integrable models. In the representative one-boson mode model considered by Cibils *et al.* [13] the integrable case was labeled by a pair of quantum numbers μ, ν where $\mu = -s, -s+1, \dots, +s$ and $\nu = 0, 1, 2, \dots$. In our model the integrable case is labeled

by three quantum numbers n_r, j, p , where n_r is the radial quantum number $n_r = 0, 1, 2, \dots$, j is the rotation quantum number $j = 1/2, 3/2, 5/2, \dots$ and p is parity, $p = \pm 1$ for gerade and ungerade states. Thus, there are two groups of states which represent a doubly degenerate set characterized by parity $p = \pm 1$. Evidently, n_r is analogous to ν , p to $s = \pm 1/2$, and j has no analog because our oscillator is two dimensional. The Hamiltonian analysis is supported by numerical evaluations of the excited energy spectra and corresponding phonon wave functions in a representation with definite parity and square of angular momentum. We choose a representation of the spectra and their probabilistic characteristics (Sec. IV) for definite j because it contains well-defined physical information. However, the real spectra and probabilistic distributions are composed of the contributions of all j 's.

In Sec. III we present approximate analytical approaches to the E \otimes e JT model for the strong and weak intercluster coupling in order to elucidate the peculiar features of the numerical excited spectra and wave functions. In particular, we find the approximate analytical form of wave functions for strongly localized ("exotic") states as well as for extended states and compare them with respective numerical results. Special interest is given to identification of the regions of the spectra with different extent of ordering, from the long-range ordered region of linear oscillations (extended states) to the short-range ordered region of localized states with dynamical avoiding (kink lattice). The dynamical Calogero-Moser approach appears to be capable of describing all three regions of the spectra: the dimerization region with pairs of oscillating levels, the kink train lattice, and the intermediate region of nonlinear fluctuations accounting for the kink nucleation phase. The intermediate region was found to exhibit quantum chaotic behavior under certain conditions. Section IV complements the dynamical insight by that based on statistical properties of the spectra. We consider the nearest level-spacing probability distributions and probability distributions of level curvatures used as relevant statistical characteristics of complex spectra [1, 2, 21]. The particular level-spacing distributions for fixed rotation quantum numbers are believed to be the most informative, since they behave very specifically for different parts of the spectra, reflecting their specific dynamic behavior.

II. HAMILTONIAN AND EQUATIONS FOR EXCITED SPECTRUM

We investigate local spinless double degenerate electron states linearly coupled to two intramolecular phonon (vibron) modes described by Hamiltonian

$$H = (b_1^\dagger b_1 + b_2^\dagger b_2 + 1)I + \alpha(b_1^\dagger + b_1)\sigma_z - \beta(b_2^\dagger + b_2)\sigma_x, \quad (1)$$

where $\sigma_x = \begin{pmatrix} 0 & 1 \\ 1 & 0 \end{pmatrix}$, $\sigma_y = i \begin{pmatrix} 0 & -1 \\ 1 & 0 \end{pmatrix}$, $\sigma_z = \begin{pmatrix} 1 & 0 \\ 0 & -1 \end{pmatrix}$ are Pauli matrices, I is the unit matrix. This pseudospin

notation refers to two-level one-electron (spinless) system.

For general $\alpha \neq \beta$ the Hamiltonian possesses a special $SU(2)$ symmetry with the reflection operator \hat{R} acting on phonon and electron subspace:

$$\hat{R} = R_{el}R_{ph}, \quad R_{el} = \sigma_x, \quad R_{ph} = \exp(i\pi b_1^\dagger b_1) \quad (2)$$

and $R_{ph}Q_1 = -Q_1R_{ph}$, $R_{ph}Q_2 = Q_2R_{ph}$; i.e., phonon 1 is antisymmetric and phonon 2 symmetric against the reflection. Then, $[R, H] = 0$ and the eigenstates can be cast as eigenfunctions of the reflection operator with eigenvalues ± 1 which are good quantum numbers.

If $\alpha = \beta$, the Hamiltonian becomes rotationally symmetric in the plane ($Q_1 \times Q_2$) and there arises another good quantum number, the eigenvalue of angular momentum \hat{J} which in fact is nothing but the infinitesimal generator of the rotational group:

$$\hat{J} = i(b_1 b_2^\dagger - b_1^\dagger b_2) - \frac{1}{2}\sigma_y. \quad (3)$$

Therefore, in the vicinity of the symmetric JT case it is feasible to cast the solutions in the form respecting this rotational symmetry. To account accurately for the group properties of the Hamiltonian one introduces radial coordinates in the $Q_1 \times Q_2$ plane $Q_1 = r \cos \phi$, $Q_2 = r \sin \phi$. The angular momentum operator (3) is

$$\hat{J} = -i \frac{\partial}{\partial \phi} - \frac{1}{2}\sigma_y,$$

and the phonon part R_{ph} of the reflection operator (2) acts as $R_{ph}(r, \phi)f(r, \phi) = f(r, \pi - \phi)$ on some $f(r, \phi)$ affecting only the ϕ coordinate. The eigenfunctions of the angular momentum operator with eigenvalue j (i.e., $\hat{J}\Psi = j\Psi$) can be set as follows:

$$\Psi_j = f_1(r) \cdot |+\rangle e^{i\phi(j-\frac{1}{2})} + f_2(r) \cdot |-\rangle e^{i\phi(j+\frac{1}{2})}, \quad (4)$$

with arbitrary $f_1(r), f_2(r)$ to be determined below. Electronic wavefunctions are expressed as

$$|+\rangle = \frac{1}{2} \begin{pmatrix} 1+i \\ 1-i \end{pmatrix}, \quad |-\rangle = \frac{1}{2} \begin{pmatrix} 1-i \\ 1+i \end{pmatrix}.$$

The angular quantum number j takes on the values $j = \pm 1/2, \pm 3/2, \pm 5/2, \dots$. The operator \hat{J} does not commute with the reflection operator \hat{R} , but \hat{J}^2 does, so it is more convenient to build solutions as joint eigenfunctions of \hat{R} and \hat{J}^2 rather than \hat{J} .

In order to make use of the reflection property of the Hamiltonian we perform the custom Fulton-Gouterman transformation [22] by means of the operator \hat{U} :

$$\hat{U} = \frac{1}{\sqrt{2}} \begin{pmatrix} 1 & R_{ph} \\ 1 & -R_{ph} \end{pmatrix}. \quad (5)$$

The resulting Hamiltonian is diagonal in electronic space and is represented in its full form as follows:

$$\begin{aligned} \tilde{H} \equiv \hat{U} \hat{H} \hat{U}^{-1} &= H_r - \frac{1}{2r^2} \cdot \frac{\partial^2}{\partial \phi^2} \\ &+ \sqrt{2}\alpha r \cdot \begin{pmatrix} \cos \phi - \sin \phi R_{ph} & 0 \\ 0 & \cos \phi + \sin \phi R_{ph} \end{pmatrix} \\ &+ (\alpha - \beta)\sqrt{2}r \cdot \begin{pmatrix} \sin \phi R_{ph} & 0 \\ 0 & -\sin \phi R_{ph} \end{pmatrix}, \end{aligned} \quad (6)$$

where

$$H_r = -\frac{1}{2r} \frac{\partial}{\partial r} \left(r \frac{\partial}{\partial r} \right) + \frac{1}{2} r^2 \quad (7)$$

is the radial part and R_{ph} , Eq.(2) is the (highly nonlinear) phonon reflection operator in the radial coordinates. In Eq. (6) we extracted explicitly the last term $\sim (\alpha - \beta)$ which breaks the rotational symmetry of the problem. Just for reference we mention the corresponding transformation of the angular momentum and its square:

$$\tilde{J} = -i \frac{\partial}{\partial \phi} \sigma_x + \frac{1}{2} \sigma_y R_{ph}. \quad (8)$$

$$\tilde{J}^2 = \left(-\frac{\partial^2}{\partial \phi^2} + \frac{1}{4} \right) + \frac{\partial}{\partial \phi} \sigma_z R_{ph}. \quad (9)$$

The transformed electron reflection operator is of course, trivial *per constructionem*, $\tilde{R}_{el} = \sigma_z$.

Although the $E \otimes E$ JT model ($\alpha = \beta$) was treated for the first time by Longuet-Higgins *et al.* [23] a long time ago, we present briefly the solution using another representation of the states. This representation enables us to distinguish the extended and "exotic" (localized) states, as we explain in Sec.III. The case $\alpha \neq \beta$ can be included on equal footing. The wave functions we are concerning with have definite parity ± 1 and square of angular momentum j^2 . Let us denote $K = \exp(i\pi(j - 1/2)) = \pm 1$.

i) In the case $K = +1$ ($j - 1/2 = 0, 2, 4, 6, \dots; -2, -4, \dots$) the *gerade* solutions read as

$$\begin{aligned} \tilde{\Psi} = \begin{pmatrix} 1 \\ 0 \end{pmatrix} \sum_{i=1,2} \frac{f_i(r)}{2\pi} \left[\sin \left(j + \frac{1}{2}(-1)^i \right) \phi \right. \\ \left. - \cos \left(j + \frac{1}{2}(-1)^i \right) \phi \right]. \end{aligned} \quad (10)$$

We shall refer to the angular wave functions in (10) as $|\pm\rangle \equiv \frac{1}{2\pi} [\sin((j + \frac{1}{2}(-1)^i)\phi) \mp \cos((j + \frac{1}{2}(-1)^i)\phi)]$.

ii) In the case $K = -1$ ($j - 1/2 = 1, 3, 5, 7, \dots; -1, -3, \dots$) we have the expression similar to (10) but with the + sign in the square bracket.

The *ungerade* case can be recovered if one takes the vector $\begin{pmatrix} 0 \\ 1 \end{pmatrix}$ instead of $\begin{pmatrix} 1 \\ 0 \end{pmatrix}$. We limit ourselves to the

case of *gerade* parity that is, in the representation (6) we are to take the upper row of the matrices.

The secular equations for the vibronic part (functions $f_1(r), f_2(r)$) in both cases are

$$H_r f_i + \frac{1}{2r^2} \left(j + \frac{1}{2}(-1)^i \right)^2 f_i + \alpha \sqrt{2} r f_k = E f_i, \quad i \neq k, \quad i, k = 1, 2, \quad (11)$$

where the radial part H_r is given by (7).

In the case $\alpha = \beta = 0$ the problem is exactly that of two independent oscillators and its solution in terms of special functions is well known. Thus, the solutions are grouped according to the $|j|$ value ($j = 1/2, 3/2, 5/2, \dots$; the parity is $+1$, as before). Within the same j the functions are divided into two groups,

(a) States with $f_2 = 0$ and

$$\begin{aligned} f_1 &\equiv \Phi^+(n_r, j; r) \\ &= \frac{1}{\sqrt{C_{n_r, j}^+}} \exp\left(-\frac{r^2}{2}\right) \cdot r^{|j-1/2|} \cdot {}_1F_1\left(-n_r, 1 + \left|j - \frac{1}{2}\right|, r^2\right), \end{aligned} \quad (12)$$

where n_r ("radial" quantum number) takes on positive integer values $n_r = 0, 1, 2, \dots$; ${}_1F_1(a, b, z)$ is a confluent hypergeometric function [satisfying equation $zy'' + (b - z)y' - ay = 0$], and the norm is

$$\frac{1}{C_{n_r, j}^+} = \frac{(|j - \frac{1}{2}|)!}{2} \cdot \frac{1}{C_{|j-1/2|}^{n_r + |j-1/2|}} \quad (13)$$

(here $C_n^m \equiv n!/[m!(n-m)!]$ is a common combinatorial factor). We label these states by + as they correspond to the $|+\rangle$ -function of the angular momentum. The product of two radial functions is defined as $\int_0^\infty r \Phi(n_r, j, r) \Phi(n_r, j, r) dr$. The energy spectrum is $E^+ = 2n_r + |j - 1/2| + 1$, and the "main" quantum number is therefore $n = 2n_r + |j - 1/2|$.

(b) States with $f_1=0$ and $f_2 \equiv \Phi^{(-)}(n_r, j; r)$ and energy $E^- = 2n_r + |j + \frac{1}{2}| + 1$ are given by the same expression as (12) but with $j + 1/2$ instead of $j - 1/2$. We refer to these states as $|-\rangle$ states.

The two groups mentioned correspond to two initially degenerate electron levels; these states are coupled together by means of the strongly nonlinear transformation involving the reflection operator $R(r, \phi)$; thus, the situation is similar to the Foulton-Gouterman treatment in ordinary phonon coordinates, where the nonlinear reflection operator coupled the phonon states pertaining to the lower and upper electron level [18].

Writing secular equations for the problem with $\alpha \neq 0$ is straightforward. The solution is sought as $f_1 = \sum_{n_r} a_{n_r} \Phi_{n_r}^+$, $f_2 = \sum_{n_r} b_{n_r} \Phi_{n_r}^-$, or, in unified notation, $f = \sum_{n=0}^\infty c_n \Phi_n$, where $\{c_n\} \equiv \{a_0, b_0, a_1, b_1, a_2, b_2, a_3, \dots\}$,

and

$$\Phi_n = \begin{cases} \Phi^+(n_r, j, r), & n = 2n_r, \\ \Phi^-(n_r, j, r), & n = 2n_r + 1. \end{cases} \quad (14)$$

The only non-zero off-diagonal elements are

$$f_{n_r, n_r} \equiv \sqrt{2} \int \Phi_{n_r}^+ \Phi_{n_r}^- r \cdot r dr = \sqrt{2} \sqrt{n_r + 1 + \left| j - \frac{1}{2} \right|} \quad (15)$$

$$f_{n_r+1, n_r} \equiv \sqrt{2} \int \Phi_{n_r+1}^+ \Phi_{n_r}^- r \cdot r dr = -\sqrt{2} \sqrt{n_r + 1} \quad (16)$$

Therefore, the secular equation acquires the familiar tridiagonal form ($E^{(0)}$ is "unperturbed" energy for the corresponding n, j),

$$\begin{aligned} c_n E_n^{(0)} + \alpha(c_{n+1} f_{n_r, n_r} + c_{n-1} f_{n_r, n_r-1}) &= E c_n, & n = 2n_r, & (17) \\ c_n E_n^{(0)} + \alpha(c_{n-1} f_{n_r, n_r} + c_{n+1} f_{n_r+1, n_r}) &= E c_n, & n = 2n_r + 1, & (18) \end{aligned}$$

with off-diagonal coefficients given by Eqs. (15) and (16). The asymmetry of the coefficients with increasing j is crucial for the appearance of nonlinear effects in spectral properties of the model. We remark by passing that Eqs. (15) and (16) differ from those given in [23] by the "minus" sign near $f_{n+1, n}$. Changing this sign to plus means merely redefinition of the base wave functions (every even base function acquires the opposite sign) and does not affect the energy spectrum. In the following it will be more convenient to use the + sign of both expressions (15) and (16).

By numerical diagonalization of the system (17) and (18) we obtain the phonon excited energy spectrum as function of α (we have taken n up to ~ 1200), as well as the corresponding wave functions. Figure 1 shows examples of the spectrum as function of α for $j = 19/2, 255/2$. The sample numerical wave functions χ_n of a few excited states of (1) are shown in Figs. 2 and 3. Figure 2 presents the wave functions χ_n in phonon coordinate representation (in the plane $Q_1 \times Q_2$), while Fig. 3 shows the projection $\chi_{n,m} \equiv |\langle \chi_n | \Phi_m^0 \rangle|^2$ of the exact numerical wave functions on the unperturbed ($\alpha = 0$) states of the radial oscillator (12) [24]. The right-hand side of Fig. 4 visualizes the whole picture of wavefunctions at a given α, j by assigning to each state $\vec{C}^{(n)} \equiv \{C_1, C_2, \dots, C_m, \dots\}$ the spectral entropy $S = -\sum_m C_m^2 \log C_m^2$ (which gives the width of the wavefunction in the representation of Fig. 3).

One remarkable feature of excited states in JT models (both rotation symmetric and that with broken rotation symmetry) are strongly localized ("exotic" [3]) states emerging abruptly between more extended ones. These states are exemplified in Fig. 2 ($n = 61, 63$) and in Fig. 3 ($n = 58$ for $j = 19/2$). The localization of those states is remarkable in comparison with neighboring or even lower-lying ones (like $n = 38, 62$ from Fig.2 compared to $n = 61, 63$).

There is an intimate relation between the position of localized states and spectral picture of levels (Fig.1).

Closer inspection [see the insets of Figs. 1(a),1(b)] shows that each and every energy level taken for a given j is avoided. Varying the parameter α infinitesimally slowly will cause the system to follow one and the same adiabatic level. But on larger scale the spectra of Fig.1 show two sets of "diabatic" lines [2] (directed upwards and downwards) which reflect a different behavior of the two main wells of the effective potential [18] when changing α . From the right-hand side of Fig.4 it is possible to note that the states for large α, j are grouped into two separated branches and the domain of localized states with small spectral entropy emerges at a critical energy corresponding to the appearance of the upper sheet of the effective potential. If one varies the parameter α fast enough the system will follow the "diabatic" lines changing the energy level number so that its wave function remains almost untouched which means that the system resides on the corresponding sheet of effective potential. All "exotic" states appear to pertain to the directed upwards diabatic lines of the spectrum seen markedly in Fig. 1. The multitude of avoided crossings (and therefore the domain referred to as "quantum chaotic") is thus formed in the intermediate energy region where these two "phases" coexist— that is above the first (lowest) diabatic line. It is clearly seen in Fig. 1(b) for large values of the angular momentum number j , while for small values of j these exotic states, although still existing, do not come into complex interplay with the ordered states. This picture is in agreement with the semiclassical treatment of the problem where the classically chaotic region is known to emerge sharply above some critical energy.

III. ANALYTICAL QUANTUM TREATMENT

A. Strong-coupling approximation: "Exotic" states

The peculiarities of the spectra shown in Fig. 1 as well as their connection to the character of pertaining wave functions (Figs. 2 and 3) can be understood from merely a rough approximation to the set of equations (17) and (18) in the following way. From Eqs. (15) and (16), for $|j| \gg n_r$, there holds $|f_{n_r, n_r}| \gg |f_{n_r+1, n_r}|$, and the basis functions in Eqs.(17) and (18) appear to be "clustered" in the sense that the coefficients C_{2n_r} and C_{2n_r+1} pertaining to the same n_r are coupled together (through f_{n_r, n_r}) essentially more strongly than to neighboring elements. [In order to avoid confusion we note that the terms "strong-" and "weak-coupling-approximation" for this section are not meant in the usual sense of large and small values of the parameter α but refer to the relative coupling inside and between the "clusters" (C_{2n}, C_{2n+1}). They are determined by the relation between f_{nn} and $f_{n+1, n}$ — i.e., by the relative values of quantum numbers j and n]. Therefore, for the zeroth approximation of strong coupling $f_{n+1, n} = 0$, and the reduced version of Eqs. (17) and (18) for each n_r gives us two sets of localized solu-

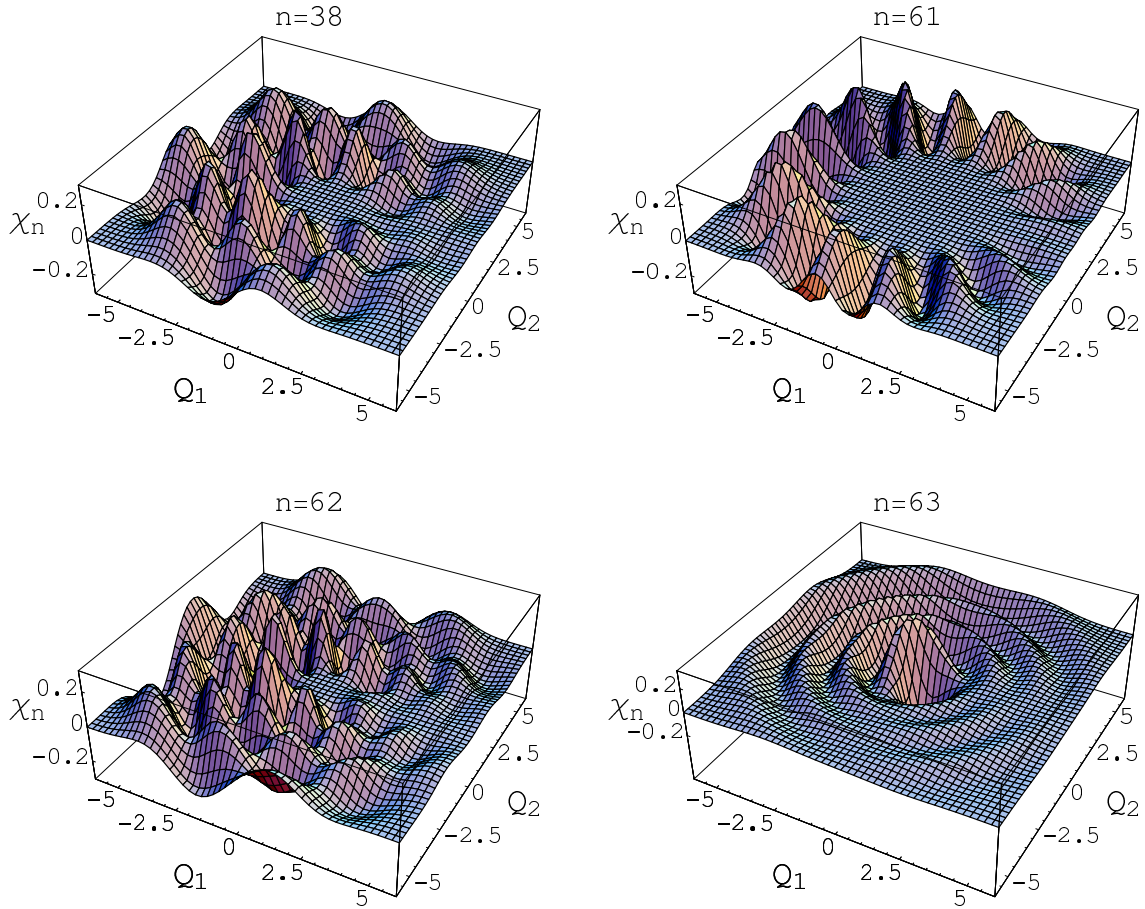


FIG. 2: (Color online) Numerical wave functions χ_n in the plane $Q_1 \times Q_2$, $\alpha = \beta = 2$. States $n=61$ and 63 are localized ("exotic").

tions for the energy

$$E_{n_r, j}(\alpha) = 2n_r + |j - 1/2| + 3/2 \pm \sqrt{2(n_r + 1 + |j - 1/2|)\alpha}, \quad (19)$$

with corresponding localized eigenvectors $C_{2n_r+1} \simeq C_{2n_r}$ (+ sign) and $C_{2n_r+1} \simeq -C_{2n_r}$ (- sign), the other C_n being zero. From Fig. 1 we can conclude that the slopes of the corresponding lines follow the predictions given by Eq.(19). This is valid for several lower clusters with small n_r which show up as directed upwards and downwards "diabatic" lines. At higher n_r , when $j \leq n_r$ the intercluster $f_{n_r+1n_r}$ and inside-cluster elements $|f_{n_r n_r}|$ become comparable and the long-range correlations yield the extended wavelike solutions seen in the upper parts of spectra in Figs. 1(a) and 1(b) [cf. inset of Fig.1(a)].

To find the form of localized wavefunctions along the diabatic line we proceed by treating terms with f_{n+1n} as perturbation to the zeroth-order solution (19). This approximation is valid far from the points of avoided crossing where the wave functions are essentially localized and unaffected by neighbors. Let us denote $\delta E \equiv E - E_m^*$ where E_m^* is the zeroth-order strong-coupling solution (19) for a given m and use the strong-coupling ansatz $C_0 = C_1, \dots, C_{2n} = C_{2n+1}$. The sum of Eqs.(17) and

(18) then yields

$$n_r = 0, 1, \dots \\ [2(n-m) + \alpha(f_{nn} - f_{mm})]C_{2n} + \frac{\sqrt{2}}{2}\alpha(\sqrt{n+1}C_{2n+2} + \sqrt{n}C_{2n-1}) = \delta E C_{2n} \quad (20)$$

Further, let us *formally* mark the cluster (C_{2n}, C_{2n+1}) as $|n\rangle$ and introduce formal creation and annihilation boson operators \hat{b}^+ and \hat{b} acting on these clusters. Since $j \gg n$, the term $f_{nn} - f_{mm}$ can be simplified by keeping only the leading-order term $\sim (n-m)$. Then the effective Hamiltonian equation in strong-coupling approximation is $(n|n)$ is replaced by $b^+b|n\rangle$

$$\left[\Omega_{eff}^{(+)} b^+ b + \frac{1}{\sqrt{2}} \alpha (\hat{b}^+ + \hat{b}) \right] |n\rangle = (\delta E_n + \Omega_{eff}^{(+)} m) |n\rangle, \quad (21)$$

with

$$\Omega_{eff}^{(+)} \equiv 2 + \alpha/\sqrt{2j-1}. \quad (22)$$

The resulting system presents a quantum oscillator displaced by the term $\alpha/\sqrt{2}$. The effect of nonlinear fluctuations is reflected in the *squeezing of its effective frequency* (22) due to j down to its minimum $\Omega_{eff}^{(+)} \rightarrow 2$

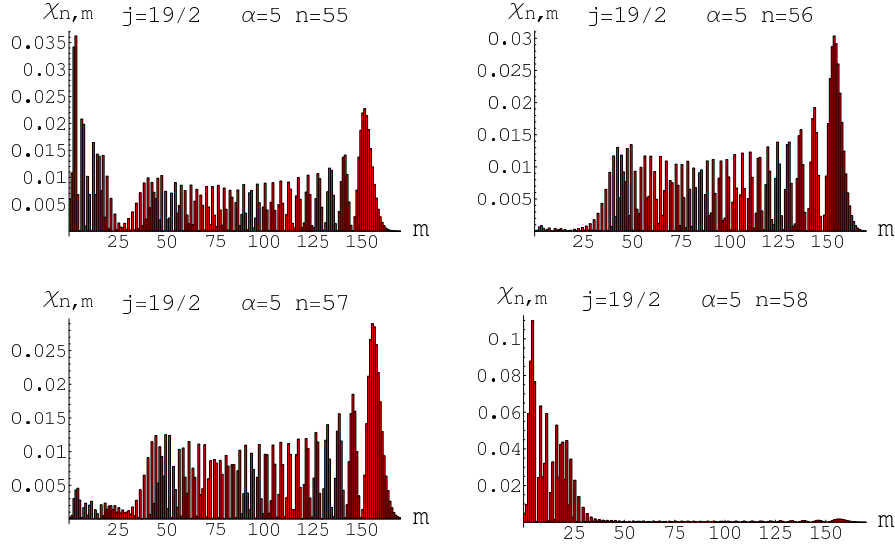


FIG. 3: (Color online) Projections of exact symmetric ($\beta = \alpha$) states χ_n on the harmonic oscillator base, $\chi_{n,m} = |\langle \chi_n | \Phi_m^0 \rangle|^2$.

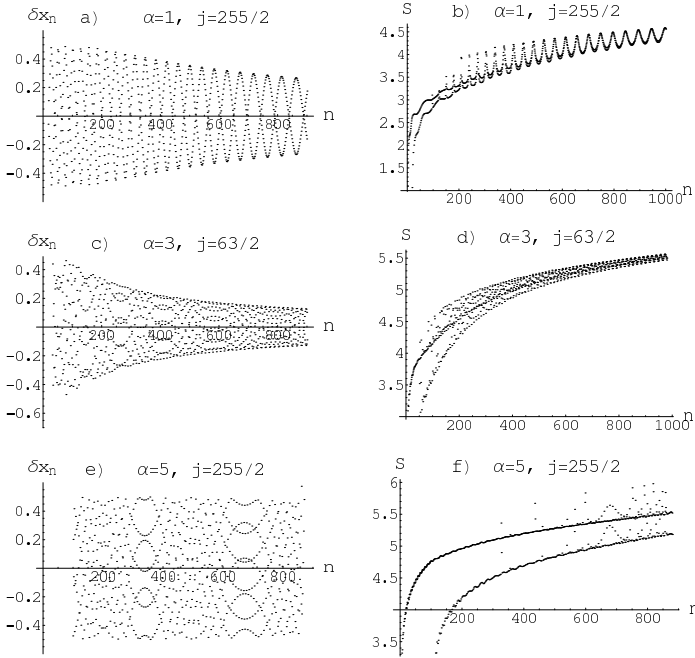


FIG. 4: Reduced energies (see text) and spectral entropies of wave functions χ_n for different couplings α and j .

in the quantum limit $j \rightarrow \infty$. The term with m in fact labels the "sites" of a pseudolattice. In this approximation the solutions for different m are translation invariant. The subsequent solutions of Eq.(21) are obtained in a standard fashion applying the displacement operator $D(\gamma) \equiv \exp(\gamma(\hat{b}^+ - \hat{b}))$, $\gamma = -\alpha/(\sqrt{2}\Omega_{eff}^{(+)})$ on the clustered pseudostates $|n\rangle \equiv (C_{2n}, C_{2n+1})$, giving the localized functions on subsequent diabatic lines (for example, for $j = 255/2$ and $\alpha = 2$ the lowest states of this fictitious oscillator correspond to wave functions with levels

$n = 37, 39, 41, 43, 45, 48, \dots$; such exact wave function is exemplified in Fig. 3 for $n = 58$). We performed an extended comparison of the exact wave functions to those found via this method in a wide range of parameters α and j . Our calculations show that the solutions of Eq.(21) yield a very plausible approximation to the exact solutions of Eqs.(17) and (18) for localized states, especially for big j : for example, for several lowest diabatic states the projection $\langle \Phi | \Psi \rangle$ of the approximate over the exact state for $j = 255/2$ lies within $0.999 - 0.995$. The same method is also suitable for approximate solutions found for several strong-coupled extended states, but there the cluster ansatz is antisymmetric, $C_{2n+1} = -C_{2n}$. The corresponding equation differs from Eq.(20) by the $-$ sign near both terms with α , respectively; there appear the $-$ sign of α in Eq.(21) and in the definition of $\Omega_{eff}^{(-)}$

$$\Omega_{eff}^{(-)} \equiv 2 - \alpha/\sqrt{2j-1}, \quad (23)$$

which is now *antisqueezed* due to nonlinear fluctuations. In the limit $j \rightarrow \infty$ both oscillators degenerate at frequency 2 and so the intercluster interaction effectively vanishes. In the absence of the intercluster interaction the energy lines from different clusters would regularly cross. The intercluster interaction leads to the spreading of the localized wavefunctions as described above and to the splitting of levels (avoided crossings). In the vicinity of an avoiding crossing we can approximately represent the relevant Hamiltonian as an effective (2×2) matrix:

$$\hat{H} = \begin{pmatrix} p\tau & u \\ u & 0 \end{pmatrix}, \quad (24)$$

where $\tau = \alpha - \alpha_0$, α_0 is the point of level collision if there were no interaction. The matrix (24) accounts for the collision of two levels, one lying at $E = 0$ (if $\tau = \pm\infty$)

and the other moving asymptotically with velocity p with "pseudotime" τ . In the representation (24) we are in the frame of reference moving downwards with α so that the velocity of the nonexotic levels is zero. If the colliding levels are weakly affected by neighbors we can consider p and u to be approximately constants. The minimal avoided crossing at $\tau = 0$ is $2|u|$. Including other non-exotic levels (thus situated at distances $1, 2, \dots$) leads to the extension of the matrix (24) to the shape given by Eq. (2) of the paper by Gaspard *et al.* [25] and accounting for a single level moving with velocity p and crossing subsequently parallel energy levels y_1, y_2, \dots with effective interaction strengths u_1, u_2, \dots . It was shown there that for equidistant energies y_i and equal strengths u_i this system immediately gives a solution in the form of a soliton propagating with pseudotime τ through the "lattice" y_n with natural analytical predictions as to the profile of energy eigenvalues $x_n(\tau)$. This soliton like solution corresponds to our diabatic level. The parameter p equals the relative slope of exotic (diabatic) and ordinary level and can be estimated in the strong-coupling approximation using Eq.(19); for the first diabatic line, it therefore holds $p \simeq 2\sqrt{2j}$. In the same approximation the level splitting (parameter u) can be estimated as $\langle \Psi_n | \hat{H}(\alpha_0) | \Phi_m \rangle$, where \hat{H} is the exact Hamiltonian and Ψ_n, Φ_m are wave functions in the strong-coupling approximation of the localized and extended states with numbers n and m , $n = 1, 2, \dots, m = n + 1, \dots$ taken in the point α_0 of crossing of the corresponding unperturbed levels. For example, for the first avoided crossing of the lowest diabatic line the estimation gives $u \sim 2/\sqrt{j}$. For large numbers m of subsequent collisions the gap value turns out to be approximately constant which suggests the applicability of the soliton like solution like those considered by Gaspard *et al.* [25].

B. Weak-coupling approximation

This is the case opposite to the previous one and valid for $j \ll n_r$. Rewrite the system (17) and (18) with coefficients (15) and (16) with positive signs in the following way (here we again label by n instead of n_r):

$$\begin{cases} C_{2n}(E_{2n}^0 - E) + \alpha [C_{2n+1}\sqrt{2n+1} + C_{2n-1}\sqrt{2n}] + \alpha C_{2n+1}k_n = 0, \\ C_{2n+1}(E_{2n+1}^0 - E) + \alpha [C_{2n}\sqrt{2n+1} + C_{2n+2}\sqrt{2n+2}] + \alpha C_{2n}k_n = 0 \end{cases} \quad (25)$$

with

$$k_n \equiv \sqrt{2n+1} \left(\sqrt{1 + \frac{2j}{2n+1}} - 1 \right), \quad n = 0, 1, \dots \quad (26)$$

($k_n \sim j/\sqrt{2n+1} \ll 1$ if $j \ll n$). The whole system (25) is elegantly cast as $\hat{H}\Psi = E\Psi$ with

$$\hat{H} = \hat{b}^+ \hat{b} + \alpha (\hat{b}^+ + \hat{b}) + \delta \hat{V} \equiv \hat{H}_0 + \delta \hat{V} \quad (27)$$

with *formal* notations: $C_{2n} \rightarrow |2n\rangle$ and $C_{2n+1} \rightarrow |2n+1\rangle$ and operators \hat{b}^+, \hat{b} acting upon our radial functions $|n\rangle$ as ordinary creation and annihilation operators [in the previous subsection the corresponding "pseudostates" referred to the cluster (C_{2n}, C_{2n+1})]; the perturbation operator $\delta \hat{V}$ acts according to the recipe:

$$\delta \hat{V} \begin{Bmatrix} |2n\rangle \\ |2n+1\rangle \end{Bmatrix} = \alpha k_n \cdot \begin{Bmatrix} |2n+1\rangle \\ |2n\rangle \end{Bmatrix} \quad (28)$$

The interaction (28) ties together the elements inside the cluster (C_{2n}, C_{2n+1}) and when it becomes considerable we again recover the strong-coupling approximation of the previous section.

From Eq.(27) we immediately get the solution of the unperturbed problem $H_0\psi = E_0\psi$ in terms of the displaced Fock states by acting the coherent operator $D(\gamma) \equiv \exp(\gamma(b^+ - b))$ on our pseudostates:

$$|\Psi\rangle \equiv |\tilde{n}\rangle = D(-\alpha)|n\rangle \quad (29)$$

with unperturbed energies $E_{\tilde{n}}^{(0)} = n - \alpha^2$. Therefore it is reasonable to investigate the reduced spectrum from which the "secular parts" of energies are subtracted: $\delta x_n \equiv E_n - n + \alpha^2 - (j - 1/2)$. On the left-hand side of Fig. 4 we plot the reduced wavelike spectrum δx_n as function of n for typical values of α, j . Examining Fig. 4 we observe that extracting the secular part reveals patterns which have not been noticed on the normal scale of the wavelike spectrum. The most interesting peculiarity is thus a crossover from two twisting quasi-sinusoids for large n and/or small α to the pictures which curiously resemble chaotic intermittent patterns containing rather characteristic windows of a regular motion. The cutoffs on the left parts of the spectra (small n) correspond to the first diabatic line below which such a reduction loses its sense since the perturbation $\delta \hat{V}$ can no more be considered as small compared to H_0 .

The standard perturbation scheme applied to (27) gives up to the first perturbation order the expression for the spectral energies the notation \tilde{n} merely reminds one of the fact that the base functions are now "displaced Fock states" (29) not to be confused with $|n\rangle$

$$E_{\tilde{n}} = \tilde{n} - \alpha^2 + \delta V_{\tilde{n}\tilde{n}} + \dots \quad (30)$$

$$\delta V_{\tilde{n}\tilde{n}} = \sum_{h,s} \langle \tilde{n} | h \rangle \langle h | \delta \hat{V} | s \rangle \langle s | \tilde{n} \rangle$$

$$= 2\alpha \sum_{h=0}^{\infty} \langle 2h+1 | D(-\alpha) | n \rangle \cdot \langle 2h | D(-\alpha) | n \rangle \cdot k_h, \quad (31)$$

where k_n is defined by (26). The matrix elements $\langle n | \tilde{m} \rangle \equiv \langle n | D(\beta) | m \rangle$ can be calculated directly:

$$\langle n | D(\beta) | m \rangle = \exp\left(-\frac{\beta^2}{2}\right) \beta^{|n-m|} \frac{\text{sgn}(n-m)}{\sqrt{m!n!}} L_{\min(n,m)}^{|n-m|}(\beta^2), \quad (32)$$

where $L_a^b(x)$ are Laguerre polynomials.

In the scope of the present paper we do not present further detailed analysis of Eq.(31), just mentioning now that it gives essentially the same structure as that presented in Fig. 4. Moreover, it can be used even for the ground state (lowest energy for given j) giving a plausible fitting for very small and very large α , although serious discrepancies occur for $\alpha \sim 1$ rendering it absolutely unsatisfactory in this region.

C. Method of level dynamics

The formalism of the generalized Calogero-Moser gas has been developed [2, 19, 20] as a useful alternative approach for Hamiltonians of the type $H = H_0 + \alpha V$ [the perturbation term linearly dependent on α ; Eq.(6) for $\alpha = \beta$ is the case with the first two terms as H_0 and the term with α as V] by mapping the eigenvalue equations on a statistical many-body system of interacting pseudoparticles. There α is a controlling parameter considered as a pseudotime, $\alpha \equiv \tau$. The eigenvalues were defined as dynamic variables $E_n(\alpha) \equiv x_n(\tau)$, $dx_n/d\tau = p_n(\tau)$. The respective classical dynamic equations for the pseudoparticles evolving in the pseudotime τ are

$$\begin{aligned} \frac{dp_n}{d\tau} &= 2 \sum_{m(\neq n)} \frac{L_{nm}L_{mn}}{(x_m - x_n)^3} \\ \frac{dL_{mn}}{d\tau} &= \sum_{l(\neq(m,n))} L_{ml}L_{ln} \left[\frac{1}{(x_n - x_l)^2} - \frac{1}{(x_m - x_l)^2} \right] \end{aligned} \quad (33)$$

where

$$\begin{aligned} p_n &\equiv \langle n(\tau)|V|n(\tau) \rangle \equiv V_{nn}, \\ L_{mn}(\tau) &= (x_n(\tau) - x_m(\tau)) \cdot V_{mn} = -L_{nm}. \end{aligned} \quad (34)$$

The system of differential equations in the form (33) is equivalent to the initial set (17) and (18) and is represented as a set of dynamical equation of motion for a gas subject to a repulsive $1/r^2$ potential ("Calogero-Moser gas"). In our case from Eqs.(15) and (16) we get (we simplify the notation, $n \equiv n_r$)

$$\begin{aligned} L_{2n2n+1} &= \sqrt{2}\sqrt{n+1+|j-1/2|} \cdot (x_{2n+1}(\tau) - x_{2n}(\tau)), \\ L_{2n-12n} &= -\sqrt{2}\sqrt{n+1} \cdot (x_{2n}(\tau) - x_{2n-1}(\tau)) \end{aligned} \quad (35)$$

The dynamic equations for a pair of even and odd coupled trajectories are then

$$\begin{aligned} \frac{dp_{2n}}{d\tau} &= 2 \frac{L_{2n2n+1} \cdot L_{2n+12n}}{(x_{2n+1} - x_{2n})^3} + 2 \frac{L_{2n2n-1} \cdot L_{2n-12n}}{(x_{2n-1} - x_{2n})^3} \\ \frac{dp_{2n+1}}{d\tau} &= 2 \frac{L_{2n+12n+2} \cdot L_{2n+22n+1}}{(x_{2n+2} - x_{2n+1})^3} + 2 \frac{L_{2n+12n} \cdot L_{2n2n+1}}{(x_{2n} - x_{2n+1})^3} \end{aligned} \quad (36)$$

For what follows we define a small fluctuation δ by $x_{2n+1} - x_{2n} \equiv 1 + \delta_{2n}$ and approximate

$(x_{2n+1} - x_{2n})^{-1} \approx 1 - \delta_{2n} + \delta_{2n}^2 - \delta_{2n}^3$. From Eqs.(35) and (36) we get the nonlinear set of equations

$$\begin{aligned} &\frac{\partial^2 \delta_{2n}}{\partial \tau^2} - v_1^2 (\delta_{2n+1} + \delta_{2n-1} - 2\delta_{2n}) \\ &= f - 4 \left| j - \frac{1}{2} \right| (\delta_{2n+1} + \delta_{2n-1}) - 4\delta_{2n-1} \\ &- 4(n+1)(\delta_{2n+1}^2 - \delta_{2n+1}^3) - 4n(\delta_{2n-1}^2 - \delta_{2n-1}^3), \quad (37) \\ &\frac{\partial^2 \delta_{2n+1}}{\partial \tau^2} - v_2^2 (\delta_{2n+2} + \delta_{2n} - 2\delta_{2n+1}) \\ &= -f + 4 \left| j - \frac{1}{2} \right| (\delta_{2n} + \delta_{2n+2}) \\ &+ 4\delta_{2n+2} - 4(\delta_{2n+2}^2 - \delta_{2n+2}^3) - 8|j-1/2|(\delta_{2n+1}^2 - \delta_{2n+1}^3) \end{aligned} \quad (38)$$

where $v_1^2 = 4(n+1+|j-1/2|)$, $v_2^2 = 4(n+1)$, and $f = 4 + 8|j-1/2|$.

For large $n \gg |j|$ and $v_1^2 \approx v_2^2$, Eqs. (37) and (38) exhibit wavelike character in n . The linear approximation to (38) bears the solution $\delta_{2n+1} \approx J_0(2\sqrt{|2j-1|n})$ where $J_0(z)$ is the Bessel function. This behavior can be recognized in the upper part of the spectra in Figs. 1(a) and 4(a). It is equivalent to the weak-coupling limit of the preceding subsection. The level avoidings in this linear part are kinematical and lead to clustering (dimerization) visualized in the level-spacing probability distributions (Sec.IV).

Equations (37) and (38) allow a useful insight into the effects of nonlinearities on the level dynamics involved. Exploiting their wavelike character we define the phase variable $\zeta = n - v\tau$ (v being an arbitrary constant velocity) and write an approximate equation for $\bar{\delta}_{2n+1} = \delta_{2n+1} - 1$ at $|j| \gg n$:

$$-(v^2 - 4|j|) \frac{\partial^2 \bar{\delta}_{2n+1}}{\partial \zeta^2} + 16|j|(\bar{\delta}_{2n+1} + \bar{\delta}_{2n+1}^2) \approx 0. \quad (39)$$

If $4|j| < v^2$, then

$$\bar{\delta}_{2n+1}(\zeta - \zeta_0) = -\frac{3}{2} \cosh^{-2} \left(\frac{(4|j|)^{1/2}}{(v^2 - 4|j|)^{1/2}} (\zeta - \zeta_0) \right). \quad (40)$$

There $\zeta_0 = n_0 - v\tau_0$ is a constant restoring the translational invariance of the solution; identifying $\partial x_{2n+1}/\partial n = 1 + \delta_{2n+1}$ we recover a soliton-shaped (kink) solution

$$\begin{aligned} x_{2n+1} &= 2n - \frac{3}{2} \frac{(v^2 - 4|j|)^{1/2}}{(4|j|)^{1/2}} \tanh \left(\frac{(4|j|)^{1/2}}{(v^2 - 4|j|)^{1/2}} (\zeta - \zeta_0) \right), \\ \zeta - \zeta_0 &= n - n_0 - v(\tau - \tau_0) \end{aligned} \quad (41)$$

corresponding to the tunneling between two adjacent levels. There, a multitude of true dynamical level avoidings results in a system of *kink trains* between subsequent pairs of levels. The limiting velocity $|v| = 2\sqrt{j}$ corresponds to the limit of vanishing fluctuation $\bar{\delta}_{2n+1}$ and thus to suppressing the tunneling.

To consider now a situation interpolating between the two previous situations we take $\delta_{2n} = \bar{\delta}_{2n} + x$ in Eq.(38) for δ_{2n} , therefore choosing x so as to eliminate the quadratic terms in Eq.(37). Let us take approximately $\delta_{2n+1} \approx \delta_{2n-1} \approx -\delta_{2n}$. Then we arrive at equation

$$\frac{1}{4} \frac{\partial^2 \bar{\delta}_{2n}}{\partial \tau^2} - n \frac{\partial^2 \bar{\delta}_{2n}}{\partial n^2} - \left(\frac{2}{3} n - 2|j| \right) \bar{\delta}_{2n} + 2n \bar{\delta}_{2n}^3 = \frac{4}{3} (2|j| - n/9). \quad (42)$$

If the oscillations in n can be neglected, under conditions for the coefficients of Eq.(42), $B \equiv 2n/3 - 2|j| > 0$ and $F \equiv (4/3)(2|j| - n/9) > 0$ (or $n > 3|j| > n/6$), there exists an exact solution [26] to (42) of periodic non-sinusoidal form spanned by F which describes the kink nucleation fluctuation. Increasing j causes the growth of the energy of the nucleus until a new kink generates. The respective solution reads

$$\bar{\delta}_{2n}(\tau) = a \frac{n_1 + \cos(2w\tau)}{n_2 + \cos(2w\tau)}, \quad (43)$$

where a, w, n_1 , and n_2 are given as

$$n_1 = (2 - n_2^2)/n_2, \quad a^2 = \frac{B}{2n} \frac{n_2^2}{2 + n_2^2}, \\ 4w^2 = 2B \frac{n_2^2 - 1}{n_2^2 + 2}, \quad a = -\frac{F}{2B} (2 + n_2^2). \quad (44)$$

From the relation $F = a(2na^2 - B)$ it is evident that the amplitude a of the fluctuation $\bar{\delta}_{2n}$ is spanned by the driving field F , growing with $|j|$ until the energy of the fluctuation reaches the energy of the kink.

Equations (37) and (38) also admit a chaotic regime for sufficiently large j, n under conditions $\partial^2 \delta_{2n} / \partial \tau^2 = 8|j - 1/2| + c_1$ and $\partial^2 \delta_{2n+1} / \partial \tau^2 = -8|j - 1/2| + c_2$, where $c_1 = c_2 = 0$, if the oscillations in n can be neglected—i.e. $\delta_{2n+1} + \delta_{2n-1} - 2\delta_{2n} \approx \partial^2 \delta_{2n} / \partial n^2 = 0$ and the same for δ_{2n+1} . One obtains then $\delta_{2n} + \delta_{2n+2} = 2n^2 \bar{\delta}_{2n+1} (1 - \bar{\delta}_{2n+1}) / [|j - 1/2|(n + j - 1/2)]$, where $\bar{\delta}_{2n+1} \equiv |j - 1/2| \delta_{2n+1} / n$. Since $\delta_{2n+2} \approx \delta_{2n}$, the famous logistic equation is recovered

$$\delta_{2n+2} \approx A \bar{\delta}_{2n+1} (1 - \bar{\delta}_{2n+1}), \quad (45)$$

where $A = n^2 / [|j - 1/2|(n + j - 1/2)]$. Equation (45) assumes the transition to the chaotic regime for $A \geq A_{crit} = 3.56994 \dots$, i.e., for

$$n_{crit} = |j - 1/2| \frac{A_{crit}}{2} \left(1 + \sqrt{1 + \frac{4}{A_{crit}}} \right) = 2.1921 \cdot |2j - 1|. \quad (46)$$

The condition $n > n_{crit}$ specifies the values of $n = n_r$ from the nonlinear region above the kink nucleation threshold $n > 3|j|$ as estimated above. On the other side the maximum value of A , $A = 4$, implies, $n_4 = (2j - 1)(1 + \sqrt{2})$, which determines the upper limit for n , $n < n_4$.

Traditionally the term “quantum chaos” is used to denote the traces of *classical* chaotic behavior at a quantum

level. As already mentioned in the Introduction, the classical counterpart of the system under consideration cannot be defined uniquely. The semiclassical approximation in two-level systems generically leads to classical chaotic patterns as a result of the nonlinear coupling between two subsystems, boson and electron, considered, respectively, as classical and quantum. The onset of classical chaos corresponds to energies above the first diabatic line. Referring to Eq. (46) it is to be emphasized that the chaotic behavior refers to mentioned a purely quantum regime of medium values of j and n_r between the weak coupling with $j \ll n_r$ (dimerized pairs of oscillators) and strong coupling with $j \gg n_r$ (kink lattice) domains. Thus, this chaotic behavior can be regarded as being of essentially quantum nature. One can conclude that the mapping of a quantum system onto the classical Calogero-Moser gas with repulsive interactions enables one to use the classical formalism for describing the system via its quantum numbers. So a promising feature of this approach is its ability to represent quantum chaos by means of classical equations.

IV. LEVEL STATISTICS

Statistical methods of investigation of the complex spectra are based on evaluation of various “chaoticity degrees” of quantum systems – i.e., the density of levels, distribution of nearest-neighbor spacings (NNS’s), and statistics of distribution of “curvatures” accounting for avoided crossings as well as more complicated measures of the distribution of avoided crossings [20, 27, 28]. Most of these characteristics can be obtained within the framework of random-matrix theory (RMT) [27, 29, 30, 31], whose predictions are supposed to adequately describe the quantum systems with generically chaotic classical analogs. However, the predictions of RMT cover in a satisfactory fashion only the “chaotic” limit of these systems, classifying them into three universality classes according to the time-reversibility of the underlying Hamiltonian [27, 29, 31] (that is, Gaussian orthogonal GOE, unitary GUE, and symplectic GSE ensembles). The fourth universality class is sometimes marked as corresponding to regular dynamics— for example, if the classical analog of the system for some values of controlling parameters exhibits mostly regular KAM trajectories.

In recent years, however, there came an understanding that chaotic patterns are to be sought not only from the energy-level distribution themselves but rather from pictures of their changing with the change of controlling parameters in the Hamiltonian (α). Thus, an alternative statistical approach is based on the concept of fully integrable description of the spectra by the dynamical model of a Calogero-Moser gas of interacting (repulsing) pseudoparticles [19, 20] where the controlling parameter is considered a pseudo-time (Section IIIC). The dynamical equations for the eigenfunctions $|x(\tau)\rangle$ of this Hamiltonian bring, for example, to the notion of level curvature

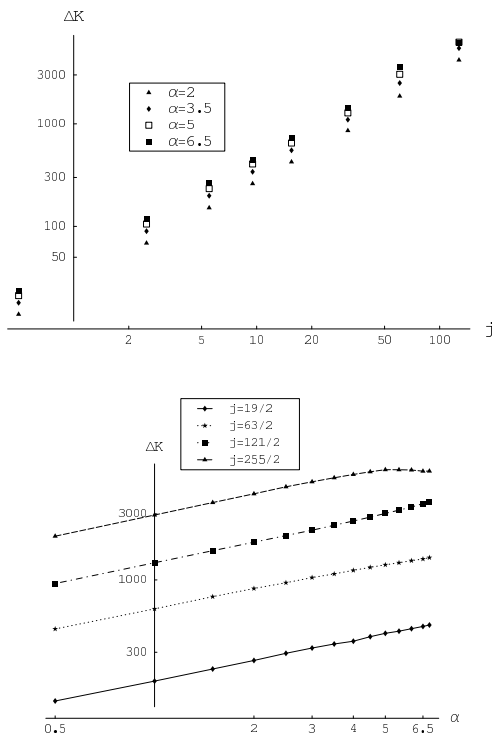


FIG. 5: The widths of curvature distributions $\Delta K \equiv \langle \Delta^2 K \rangle$ as function of j (a) and α (b). The scaling laws $\Delta K \sim j^\nu$ and $\Delta K \sim \alpha^\mu$ are seen.

$\ddot{x}(\tau)$ [20, 28] and several conjectures about its relation to the nature of the underlying RMT ensemble. Various characteristics of the level curvature distributions were reported as handy indicators of quantum chaos traces in a system. In particular, it was suggested [21] that for energy regions with quantum chaos there holds the scaling $\Delta K \sim j^\nu$ with positive ν ; meanwhile, for nonchaotic regions ν is rather negative or close to zero. We investigated the widths ΔK of the distributions of the level curvatures $P(K)$ displayed as functions of j and α [Fig. 5(a), 5(b)]. The level statistics of Fig. 5 (and of the following Fig. 6 and 7) was taken from the energy intervals above the first diabatic line where multiple avoided crossings come into being. For the improvement of statistics we used the standard recipe of collecting the level sequences from a number of α values lying in the neighborhood. Fig. 5(a) apparently shows the scaling behavior $\Delta K \sim j^\nu$ with the scaling coefficient $\nu \in (0.99 - 1.01)$ for all α . In Fig. 5(b) we observe another interesting regularity: namely, the scaling law $\Delta K \sim \alpha^\mu$ with $\mu \simeq 0.5 \pm 0.05$. This latter observation opens a challenging suggestion about the diffusive character of spreading the probability function $P(K)$ in pseudotime α . From a closer inspection of these distribution functions one can even anticipate that the resulting diffusive equation would have a telegraph term and possibly is capable of bearing anomalous diffusion patterns. We are going to return to this point elsewhere.

The realm of the symmetric JT model with definite j value is that of an effectively two-dimensional oscillator

(or rather two oscillators pertaining to two electron levels); thus, the level-spacing picture for the unperturbed problem $\alpha = 0$ is trivial: all levels of a quantum harmonic oscillator are equidistant, so $P(S) = \delta(S - 1)$. The non-trivial behavior of the NNS distribution appears to be consequence of the effective coupling of two oscillators through α . In Fig. 6 we show the level-spacing distributions $P(S)$ for a set of j with different α . Our results indicate that the most close to RMT prediction situations [RMT would yield a Wigner distribution of NNS's in the form $P(S) \sim S \exp(-S^2)$] are located at intermediate values of j and α as it is seen for pictures with $j = 63/2$. Meanwhile, the extreme values of j and α do not fit RMT at all. However, one can notice a crossover between two distinctly different types of behavior seen, for example, at $j = 63/2, \alpha = 2$ and $j = 255/2$. Such a behavior can be semiquantitatively explained on the basis of the conception of effective potential wells— for example, built on the semiclassical coherent probe function in the space of their parameters (see [18]; this variant of building an effective potential is in fact the Husimi representation of the Hamiltonian operator taken for zero values of classical momenta). Namely, the characteristic for big j is the presence of two almost noninteracting wells which are seen from the right-hand of Fig. 4 showing spectral entropies. We can assume that each of the wells refers to a separate quantum oscillator having level spacing a and b (let $a < b$). The superposition of the distribution for two independent sets of levels is found to be in the form (see for details, e.g., Berry et al[32]):

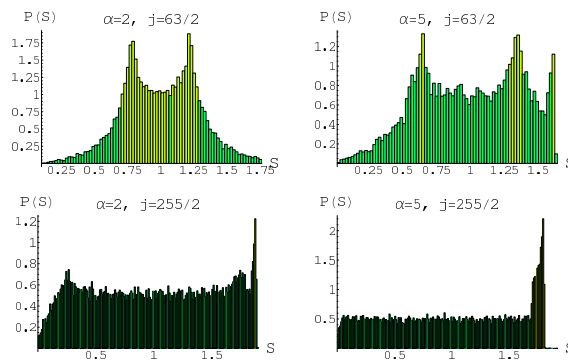


FIG. 6: (Color online) Level spacing distributions for particular j . Dimerization clustering related to two dominating level spacings is evident for $\alpha = 2$ and $j = 63/2$. The third peak from localized states occurs at large j and α , dominating close to the semiclassical limit (compare with Fig. 4). The crossover from the dimerized regime to the localized regime with increasing j and α is evident.

$$P(S) \simeq \frac{2}{b}\theta(a - S) + \delta(S - a), \quad (47)$$

θ being step function [we considered $a \ll b$; if they are comparable, a refinement to (47) is straightforward]. Conformity of Fig. 6 to the prediction (47) with $a \simeq 1.7$ and $b = 4$ for large j and α (for $j = 255/2$, $\alpha \geq 5$) is perceivable. From the “adiabatic sheet” treatment in [18] one can even define the parameters of both effective potential wells. The opposite case of small j (α) apparently indicates a dimerized structure with two dominating spacings, with increasing extent of correlation when decreasing j and α . The graphs of the M-shaped probability distributions for fixed j in Fig. 6(a) for small j and large n are similar to those by Cibils *et al.* [13] for $s = 1/2$ which corresponds to our parity $p = 1$. There, the asymmetry between the matrix elements f_{nn} and $f_{n+1,n}$ is negligible and the weak-coupling approach is satisfactory. However, for large j with large asymmetry of the matrix elements the strong-coupling limit of kink lattice is valid. There the relief of the three-minimum ground-state potential unfolds (Figs. 4) and the three-peak picture arises [Figs. 6(b) and 6(c)].

The level-spacing statistics taken separately for particular values of j is the basis of a more realistic investigation of the level statistics of the whole spectrum of the system whose Hamiltonian in this representation is a block matrix of blocks on the diagonal corresponding to definite j and off-diagonal blocks coupling [in the generalized $E \otimes (b_1 + b_2)$ JT model] for different j 's. The peculiarity of the symmetric Jahn-Teller system is that the interblock coupling is exactly zero, and as was shown already in [33] with a variant of the central limit theorem, the superposition of (infinite or very large number) independent blocks will give the cumulative distribution which must be of Poissonian character, $P(S) = \exp(-S)$. This result is exactly that obtained by Yamasaki *et al.* [17] for the absence of (trigonal) nonlinearity and which was claimed to be testimony of the absence of any traces

of quantum chaos in this case. The detailed account for the level statistics for the generalized JT model including the symmetric JT as its partial case is reported by us elsewhere [34]. For the sake of the present paper we just mention the serious deviations of the expected Poisson result in the symmetric case in the domain of dominating quantum fluctuations ($1 > (\alpha, \beta)$). Indeed, the $P(S)$ distribution shown for $\alpha = \beta = 0.5$ exhibits considerable deviations from the expected Poisson shape, showing anomalously large variance > 4 (for $\alpha = \beta = 1$ this dispersion is $\simeq 1.17$, and for the domain $1 < \alpha$ it is rather rigid, falling normally within $0.7 - 0.8$ irrespectively to the values of α). These anomalies are apparently due to the high nonuniformity of the spectral statistics in this case for different energy intervals. In Fig. 7 we show the level-spacing distributions for $\alpha = \beta = 0.5$ taken for separate level intervals (100 – 500, 500 – 1000, 1000 – 1500, and 1500 – 2000) from which this difference is apparent. The distributions with $\alpha, \beta > 1$, in contrast, are rather robust with respect to changing energy intervals.

V. CONCLUSION

The energy spectrum of a long but finite chain of correlated clusters is governed by the interplay (competition) of intracluster and intercluster interactions (repulsions) determined by two quantum numbers: rotational j and radial n_r . At small $|j|$, $|j| \ll n_r$, the excited spectrum is long-range-ordered and the broad *dimerized* region is a sample of pairwise oscillating levels. Respective level avoidings in the upper part of the spectra [the inset in Fig. 1(a)] result from the oscillations due to comparable intracluster and intercluster interactions in this part of the spectra. Such a regular wavelike spectrum is known to be characteristic for one-boson two-level systems since long time ago [35] and is a signature of the dimerization. The similarity of this part of the $E \otimes e$ spectra with two bosons to the spectra of one-boson systems was discussed in a more detail in the Introduction.

In the strong coupling limit of large j , $|j| \gg n_r$ (the intercluster interaction is small or negligible when compared to the intracluster one) there appears a *kink lattice* – i.e., the regular lattice of oscillating level clusters. There the levels are bridged by a flip (kink) up to a higher level due to the tunneling [Fig. 1(b) above the diabatic line and inset therein]. At moderate values of $|j|$ and α there appears an intermediate region of strong nonlinear fluctuations responsible for the *nucleation of the kinks* [Figs. 1, 4(c), and 4(d)].

By an approximate quantum treatment of both the strong- and weak-coupling limit in the Sec.III we have found analytically the respective wavefunctions and energies of localized exotic and extended states in a form of modified coherent oscillators: at strong coupling we showed the appearance of two branches of coherent oscillators with effective frequencies $\Omega_{eff}^{(\pm)} \equiv 2 \pm \alpha/\sqrt{2j-1}$ squeezed or antisqueezed by j to the degenerate quantum limit $\Omega = 2$ at $j \rightarrow \infty$. An excellent agreement of these solutions to the exact numerical wave functions for large j ($\geq 63/2$) was marked. In the weak-coupling limit of small $j \ll n_r$ the first order of perturbation theory yields satisfactory agreement with exact results for the wave functions except for $\alpha \sim 1$ ($\Omega \sim 1$). Therefore simple approximate analytical solutions for wave functions are available in both the strong- and weak-coupling limits corresponding to the soliton (kink) and wavelike lattice (in the plane energy-coupling parameter).

The mapping of our model on the Calogero-Moser gas of classical pseudoparticles with repulsive interactions enabled us to describe (Sec.III C) all regions of the spectra by a set of classical equations in terms of its quantum numbers. In the intermediate region the equations under certain conditions implied the logistic equation route to chaos in terms of quantum numbers.

On the other hand, the qualitative features of the excited spectra of the $E \otimes e$ Jahn-Teller model can be understood from the outline of the shape of the effective potential used for investigating the ground state of the model [18, 36]. With increasing j and α up to the semiclassical limit there emerge up to three effective potential minima. In accordance with this we identify the above-mentioned three phases in the spectra: for small coupling α the dimerized phase is related to two broad minima of the potential. Increasing α opens one additional narrow minimum (for the ground state its counterpart was responsible for emerging the "tunneling phase" or light polaron [36]). The complex interplay of wave functions located over three minima corresponds to our intermediate region [Fig. 4(c) and 4(d)] where the level statistics (Fig. 6) exhibits chaotic patterns close below the limit expected for fully chaotic RMT statistics [29]. Next, subsequently increasing α and j brings a suppression of the initial two "weak-coupling" wide minima in the quantum limit of large j . Thus there persist two almost noninteracting potential wells: a narrow and a wide one. Two remaining noninteracting branches of the spectra are markedly seen in Fig. 4(f). The lowest branch of the

spectral entropy in Fig. 4(f) is related to the (third) narrow minimum of the effective potential responsible for the kink lattice phase of avoided crossings (localized states) in energy spectra. This behavior is also supported by the shape of the level-spacing distribution [Fig. 6(d) and Eq.(47)] which has the marked character of superimposing two almost noninteracting effective oscillators with different frequencies.

The statistical level-spacing probability distributions investigated in Sec.IV were numerically calculated for particular j 's. Their features are in agreement with above conclusions based on the shape of the effective potential: They are shown to exhibit up to three maxima (Fig. 6) depending on j and α . For moderate j and α a pair of almost symmetric prominent peaks of $P(s)$ are related to two dominating strongly correlated potential wells which are getting closer at small α and j . The two dominating peaks of level spacings refer to the dimerization clustering of subsequent even and odd levels. At large j and α the NNS distributions are strictly determined by the shape of the ground-state effective potential (Fig. 6(d)). The analysis of the cumulative statistical distributions of level spacings shows a strongly changing picture of different segments of spectra especially at weak couplings (Fig. 7). The dimerized phase is pronounced in the lowest part of spectra where a strong clustering is apparent from two peaks of the level-spacing distribution $P(S)$. In the middle part of spectra some patterns of the Wigner distribution at least at large S are perceivable. The widths of the level curvature distributions were found (Fig.5) to be scaled as $\Delta K \propto j^\nu$, $\nu \propto 1$, and thus satisfying the criterion suggested [21] for indicating chaotic patterns in our quantum system. Additionally, the scaling behavior $\Delta K \propto \alpha^{0.5}$ was revealed which traces a possible bridge between mechanical and statistical points of understanding the complexity in the system referring to a possibility of reformulating the level curvature statistics stochastically, as a Calogero-Moser gas diffusing with "time" α [37].

Since the sets of levels with $j \neq j'$ for the symmetric JT system are uncorrelated (matrix elements between the states are zero), the respective levels intersect (Sec. II). The cumulative level-spacing probability distributions consist of independent contributions of all j 's and, consequently, the Poissonian distribution should supercede the above-described partial distributions. The cumulative level-spacing distributions, however, are found to exhibit enormously large dispersions $\gg 1$ at small $\alpha \leq 1$ (Fig. 7) which can be evidence for the overlapping of distributions of two kinds: a Poissonian one from the crossing of uncorrelated levels $j \neq j'$ and two-peak ones for the particular j 's described above. In the quantum limit $j \rightarrow \infty$ the spectrum tends to a continuum and the respective levels at $j \rightarrow j'$ will tend to avoiding levels.

Acknowledgement. It is a pleasure to thank Professor J. Peřina for useful discussion. This research was partially supported by Project No. 202/06/0396 of the

Grant Agency of the Czech Republic as well as by Project No. 2/6073/26 of the Grant Agency VEGA of the Slovak Academy of Sciences. One of us (S.Sh.) is also indebted for partial support by Project No. LN00A015 of the Ministry of Education of the Czech Republic as well as to the

Department of Theoretical Physics of the Faculty of Science of the Palacký University in Olomouc.

-
- [1] B. Eckhardt, Phys. Rep. **163**, 205 (1988).
- [2] K. Nakamura, *Quantum Chaos-A New Paradigm of Non-linear Dynamics* (Cambridge University Press, Cambridge, England, 1993).
- [3] H. Eiermann and M. Wagner, J. Chem. Phys. **96**, 4509 (1992).
- [4] U. Herfort and M. Wagner, J. Phys.: Condens. Matter **13**, 3297 (2001).
- [5] A. Königeter and M. Wagner, J. Chem. Phys. **92**, 4003 (1990).
- [6] R. Graham and M. Hohnerbach, Z. Phys. B:Condens.Matter **57**, 233 (1984); Phys. Lett. **101A**, 61 (1984).
- [7] J. Eidson and R. F. Fox, Phys. Rev.A **34**, 3288 (1986); R. F. Fox and J. Eidson, *ibid.* **34**, 482 (1986); **36**, 4321 (1987).
- [8] R. Blümel and B. Esser, Phys. Rev. Lett. **72**, 3658 (1994); B. Esser and H. Schanz, Z. Phys.B:Condens.Matter **96**, 553, (1995); H. Schanz and B. Esser, *ibid.* **101**, 299 (1996); Phys. Rev.A **55**, 3375 (1997).
- [9] P.I. Belobrov, G.M. Zaslavskii, and G.Kh. Tartakovskii, Zh.Eksp.Teor.Fiz **71**, 1779 (1976)[Sov.Phys.JETP **44**, 945 (1976)].
- [10] P.W. Milonni, J.R. Ackerhalt, and H.W. Galbraith, Phys. Rev. Lett. **50**, 966 (1983).
- [11] K. Furuya, M.C. Nemes, and G.Q. Pellegrino, Phys. Rev. Lett. **80**, 5524 (1998).
- [12] C.H. Lewenkopf, M.C. Nemes, V. Marvulle, M.P. Pato, and W.F. Wreszinski, Phys. Lett. A **155**, 113 (1991)
- [13] M. Cibils, Y. Cuche, and G. Müller, Z. Phys.B:Condens.Matter **97**, 565 (1995).
- [14] R. Steib, J.L. Schoendorff, H.J. Korsch, and P. Reineker, Phys. Rev. E **57**, 6534 (1998).
- [15] R. Graham and M. Hohnerbach, Phys. Rev. Lett. **57**, 1378 (1986).
- [16] M.C.M. O'Brien, Proc. R. Soc. London, Ser.A **281**, 323 (1964).
- [17] H. Yamasaki, Y. Natsume, A. Terai, and K. Nakamura, Phys. Rev.E **68**, 046201 (2003).
- [18] E. Majerníková and S. Shpyrko, J. Phys.: Condens. Matter **15**, 2137 (2003).
- [19] P. Pechukas, Phys. Rev. Lett. **51**, 943 (1983); T. Yukawa, Phys. Lett. A **116**, 227 (1986).
- [20] P. Gaspard, S.A. Rice, H.J. Mikeska, and K. Nakamura, Phys. Rev. A **42**, 4015 (1990).
- [21] K. Nakamura, Y. Nakahara, and A.R. Bishop, Phys.Rev.Lett **54**, 861 (1985); K. Nakamura and A.R. Bishop, Phys. Rev.B **33**, 1963 (1986).
- [22] H.B.Shore and L.M.Sander, Phys. Rev.B **7**, 4537 (1973).
- [23] H.C.Longuet-Higgins, U. Öpik, and M.H.L. Pryce, Proc. R. Soc. London, Ser.A **244**, 1 (1958).
- [24] Note that the numeration of states in Fig. 3 labels the states with given j , and in Fig. 2 all states are labeled in ascending order in energy (that is contain all j).
- [25] P.Gaspard, S.A.Rice, and K.Nakamura, Phys. Rev. Lett. **63**, 930 (1989).
- [26] P.Lal, Phys. Lett. **114A**, 410 (1986).
- [27] T.A.Brody, J.Flores, J.B.French, P.A.Mello, A.Pandey, and S.S.M. Wong, Rev. Mod. Phys. **53**, 385 (1981).
- [28] J. Zakrzewski and M. Kuś, Phys. Rev. Lett. **67**, 2749 (1991); J. Zakrzewski and D. Delande, Phys. Rev. E **47**, 1650 (1993); J. Zakrzewski, D. Delande, and M. Kuś, *ibid.* **47**, 1665 (1993).
- [29] F.J.Dyson, J.Math.Phys. **3**, 140 (1962); **3**, 157 (1962); **3**, 166 (1962); **3**, 1191; **3**, 1199 (1962).
- [30] F.J.Dyson, J.Math.Phys. **13**, 90 (1972).
- [31] M.L.Mehta, Nucl. Phys. **18**, 395 (1960); M.L. Mehta and M. Gaudin, *ibid.* **18** 420 (1960); M. Gaudin, *ibid.* **25**, 447 (1961).
- [32] M.V.Berry and M.Robnik, J.Phys.A **17**, (1984) 2413.
- [33] N.Rosenzweig and C.E.Porter, Phys. Rev. **120**, 1968 (1960).
- [34] E. Majerníková and S. Shpyrko, Phys.Rev.E **73**, 057202 (2006), e-print cond-mat/0510710.
- [35] M. Kuś, Phys.Rev.Lett. **54**, 1343 (1985).
- [36] E. Majerníková, J. Riedel, and S. Shpyrko, Phys.Rev.B **65**, 174305 (2002).
- [37] H.Hasegawa, H.J.Mikeska, and H.Frahm, Phys.Rev.A **38**, 395 (1988).

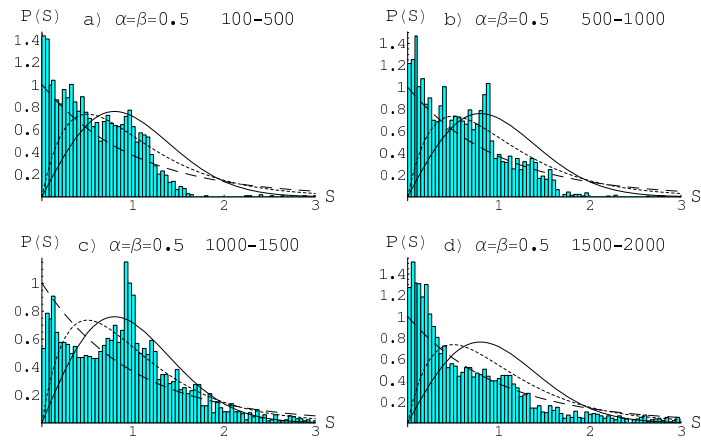


FIG. 7: (Color online) Level-spacing distributions for subsequent segments of cumulative energy spectrum for small $\alpha < 1$. Dimerization clustering peaks as remnants of the distribution in Fig. 6 are evident. The reference curves pertain to Wigner (solid line), semi-Poisson (dotted line), and Poisson (dashed line) distributions.